Further Investigations into Plasma Flow and Detachment from a Magnetic Nozzle

Mikhail Khodak, Princeton University/PPPL, Princeton, New Jersey

Project Sponsored by the U.S. Department of Energy

September 2013

Introduction:

As part of the Princeton's Field Reverse Configuration (FRC) project, plasma flow from a magnetic nozzle has been under investigation in order to gain insight into the process of detachment of charged particles from expanding magnetic field lines. A better understanding of this occurrence is important for both the exhaust system of the FRC and for electromagnetic propulsion systems, where plasma detachment is critically important for any thrust to occur. Analytically, detachment has been shown using MHD equations to occur when the local kinetic energy of particles is greater than the local magnetic field energy.[1]

This study uses LSP, a PIC code, to simulate the movement of plasma particles through a given field geometry, and compares two different ways of simulating this scenario in the code. All particles were sourced $20cm$ upstream from the nozzle throat at densities between $10^9 cm^{-3}$ and $10^{10} cm^{-3}$ and temperatures of $5eV$ for hydrogen ions and $20eV$ for electrons. One method injected ions at a velocity slightly above the sound speed and sourced electrons using Child-Langmuir emission into a two-dimensional cylindrical geometry, while the other injected both ions and electrons at their respective thermal velocities, also in two dimensions. An assessment of the three methods based on both physical results and computational load will inform further numerical work in the area, which aims to eventually simulate in production-level densities of $10^{13} cm^{-3}$.

Simulation Region and Magnetic Field Geometry

All simulations were run in cylindrical coordinates; particles were injected $20cm$ upstream from the nozzle with an input momentum in the axial direction. The expansion region, defined as the simulation space after the nozzle, extended for $160cm$ after the nozzle, although the last $40cm$ were added so that the boundary on the right border of the simulation, which was made conducting in order to resolve well with the implicit algorithm used by LSP, did not affect particle interactions in the region of interest. All other boundaries were conducting as well.

The magnetic field was numerically computed with a precision of within $1G$ and a cell spacing of $.05cm$ for two short, thick solenoids, one before the nozzle and one around the throat (Table 1). The resulting field lines were initially parallel to the z-axis, contracting right before the nozzle and then expanding afterwards (Figure 1). The field had an axial (B_z) magnitude of $850G$ at the injection and $1420G$ at the nozzle, after which point the magnitude fell off rapidly (Figure 2).

Taking any individual ion moving with parallel velocity $v_{||}$ and perpendicular velocity $v_{\perp} = r_i\omega_c$, where r_i is the gyroradius and ω_c the cyclotron frequency in this field at a location where the magnetic field strength is B, from conservation of kinetic energy in a magnetic field we have that the component velocities $v'_{||}$ and $v'_{\perp}$ at a later point in time can be related by

Table 1		
Solenoid	Injection	Nozzle
Axial Center (cm)	-.325	0.0
Length (cm)	.6	.05
Inner Radius (cm)	.1	.05
Outer Radius (cm)	.15	.1
Current (A)	120	180
Number of Turns	360	72

(1) $$v_{||}'^2 + v_{\perp}'^2 = v_{||}^2 + v_{\perp}^2 .$$

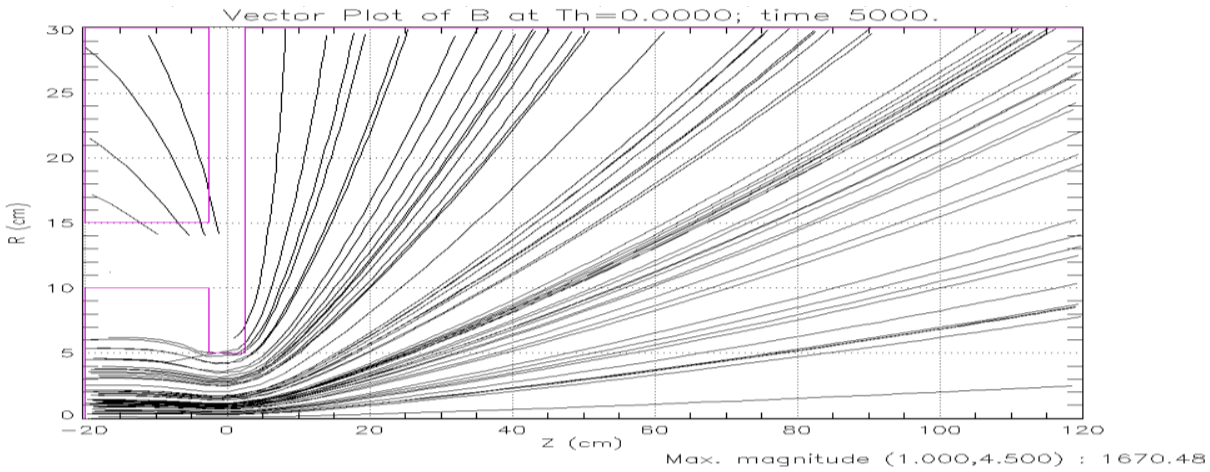

Figure 1

Also, in this cylindrically-symmetric system we can use the constancy of the magnetic moment $\mu = \frac{m}{2B}v_{\perp}^2$ to write

(2) $$\frac{v_{\perp}'^2}{B'} = \frac{v_{\perp}^2}{B} \Rightarrow v'_{\perp} = v_{\perp}\sqrt{\frac{B'}{B}},$$

where B' is the magnetic field strength at the later point in time. Given

(3) $$v_{\perp} = r_i\omega_c = 1.02 \cdot 10^2 \frac{\sqrt{T_i}}{B} * 9.58 \cdot 10^3 B = 9.7716 \cdot 10^5 \sqrt{T_i}\ \frac{cm}{s},$$

where T_i is the initial particle temperature, we can substitute into (2) to arrive at

(4) $$v'_{\perp} = 9.7716 \cdot 10^5 \sqrt{\frac{T_i B'}{B}} \frac{cm}{s},$$

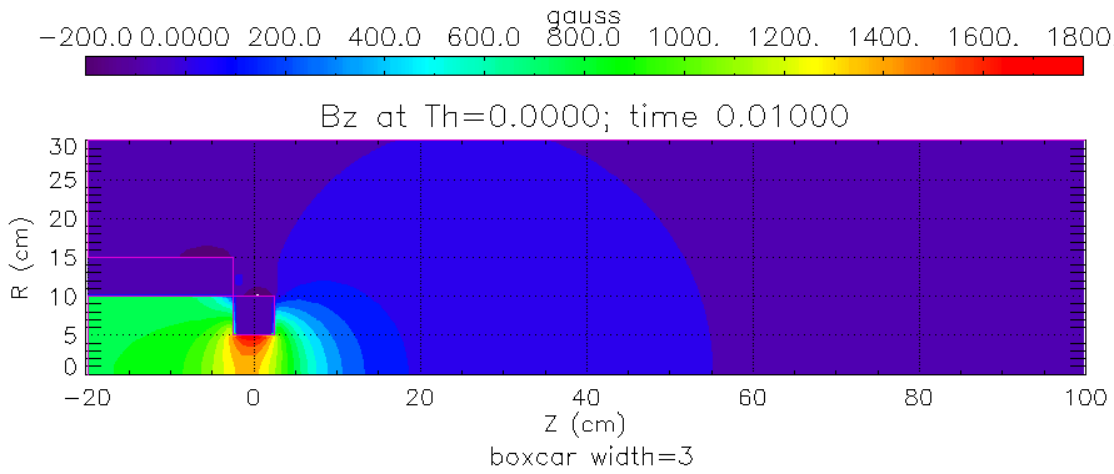

Figure 2

from which we can use (1) to predict that

(5) $$v_{||}^{\prime 2} = \left(v_{||}^2 + 9.548417 \cdot 10^{11} T_i \left(1 - \frac{B\prime}{B}\right)\right)\left(\frac{cm}{s}\right)^2.$$

So given a magnetic field strength at an initial and final location, as well as the initial parallel velocity and ion temperature, we can use (5) to predict the parallel velocity at the final location as well. In our simulations, because the ratio of the local magnetic field after the nozzle to the magnetic field at the nozzle throat is less than 1 and very small at $120cm$, we expect the plasma to accelerate along the field lines as it moves through the expansion region. If this is the case, the resulting greater kinetic energy coupled with the rapidly decreasing magnetic field energy density should lead to plasma detachment.

Case 1: Generating Electrons via Child-Langmuir Emission

In this setup, ions were injected at a density of $10^{10} cm^{-3}$ from the left end of the simulation field, at $z = -20cm$, out to a radius of 1cm. The ion density was raised to $10^{10} cm^{-3}$ over the course of $100ns$, with the initial injection at $t = 0ns$ being at a density of $10^7 cm^{-3}$. The injection momentum was set at about $6 \cdot 10^6 \frac{cm}{s}$, just above the sound speed corresponding to $20eV$ electrons, and the ions were given a temperature of $5eV$. To maintain initial quasi-neutrality, $20eV$ electrons were sourced over an area between $z = -20cm$ to $z = -19.9cm$ and also out to a radius of $1cm$. The electrons were created using Child-Langmuir field-stress, in which electrons are emitted according to the Child-Langmuir law in correspondence with the positive voltage caused by the injected ions. This creates an electron density of the same magnitude as the ion density, although the electrons do not collectively have any directed initial momentum.

In the first $100ns$, as the ion density, and therefore the electron density too, was being raised, we can see that although initially the electrons have no combined momentum, they are quickly accelerated in the positive axial direction and have already reached the expansion region, although in very low densities (Figure 3). In terms of distance traveled along the axis, however, the electron density (Figure 4) corresponds with the ion density (Figure 5) for all levels above $10^8 cm^{-3}$. In the same scalar contour plots, we can see that while electrons generally remain within the $1cm$

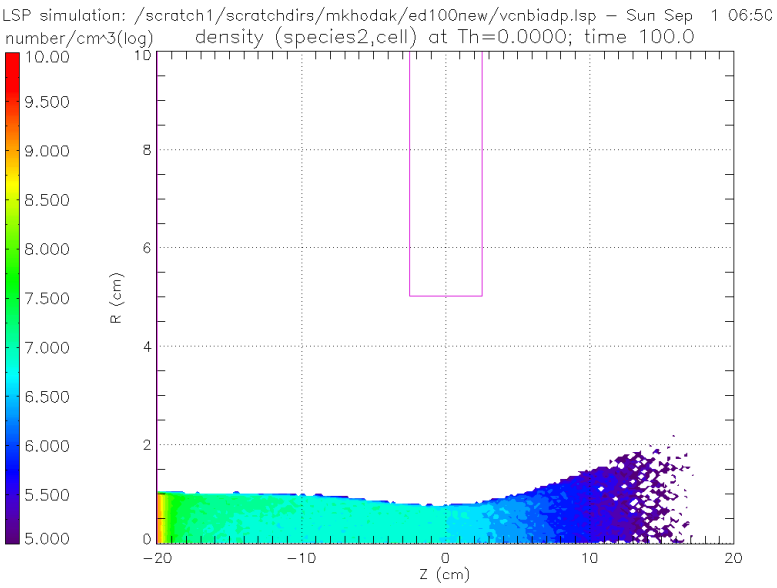

Figure 3

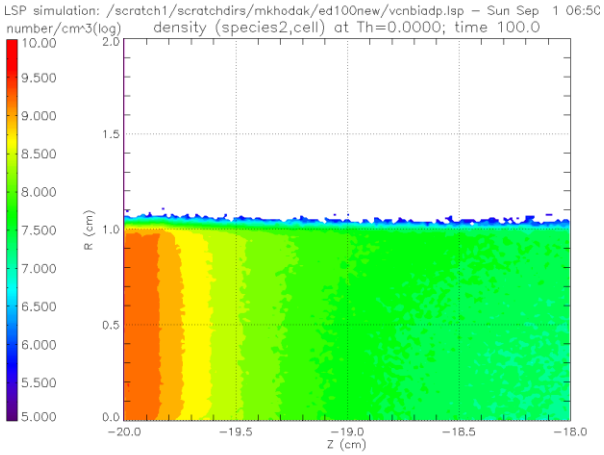

Figure 4

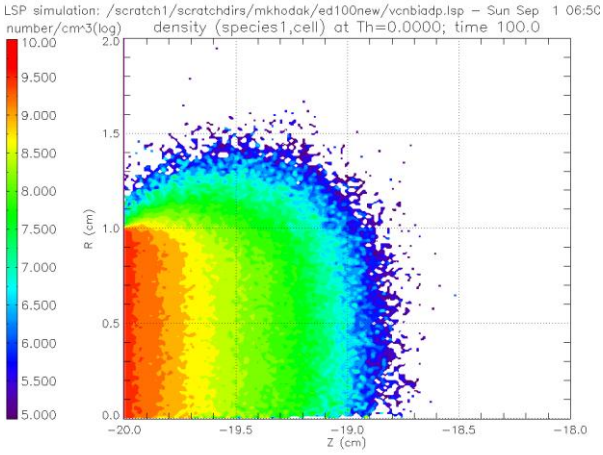

Figure 5

injection radius as they move in the positive axial direction, the ions drift out in the radial direction to $1.3cm$ in lower densities of $10^7 cm^{-3}$. This corresponds to the ion gyroradius $r_i = .3cm$ at $5eV$ in a $850G$ magnetic field compared to the electron gyroradius $r_e = .014cm$ for electrons at $20eV$ in the same field.

As the simulation progresses, the low density electrons further downstream from the

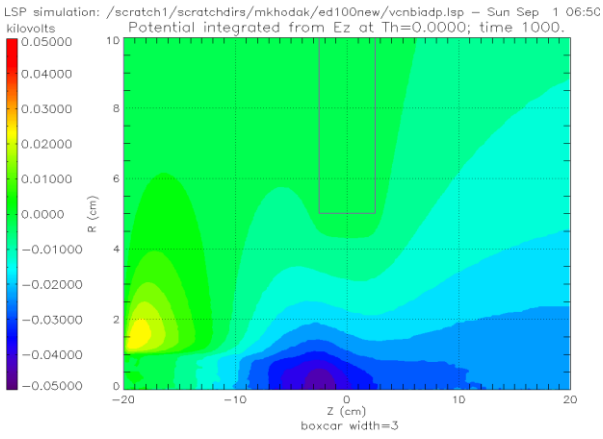

Figure 6

main density plasma create a negative potential just ahead of the ions (Figure 6). By $5\mu s$ this has accelerated some ions axially, expanding the region of low density ions (Figure 7) towards the electrons (Figure 8) even as the main body of ions at n = $10^{10}cm^{-3}$ decreases in speed due to the contracting magnetic field (Figure 9). From the velocity slice graph along the z-axis we see that the ion z-velocity, given as a fraction of c, at $z = 0cm$ is $5.78 \cdot 10^6 \frac{cm}{s}$, or just slightly above the $5.73 \cdot 10^6 \frac{cm}{s}$ that is predicted by (5) given the input velocity. However, we would expect that the minimum velocity would be at the point of strongest magnetic field, which is not the case.

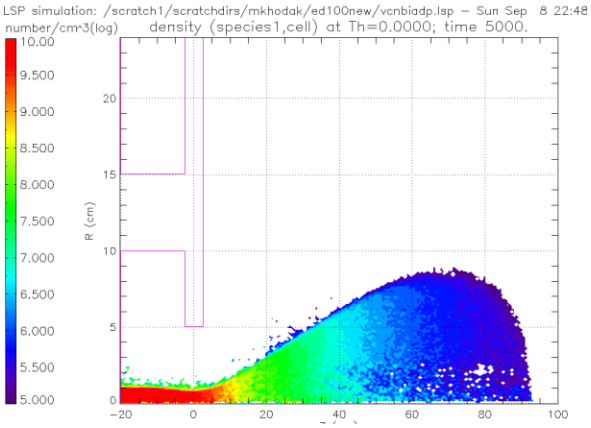

Figure 7

Figure 7 also shows that unlike the electrons, which follow the expanding field lines closely, the ions begin to move across the field lines after $z = 40cm$ in a direction more parallel to the z-axis. The simulation is being continued to see whether this seeming detachment of ions at lower densities also occurs at higher densities or when steady-state is achieved, and whether the resulting positive radial E-field will also pull electrons closer to the axis. The ions at lower densities further downstream approach speeds of $2.4 \cdot 10^7 \frac{cm}{s}$, or $300eV$, a kinetic energy which, if maintained, would point to detachment occurring (Figure 10).

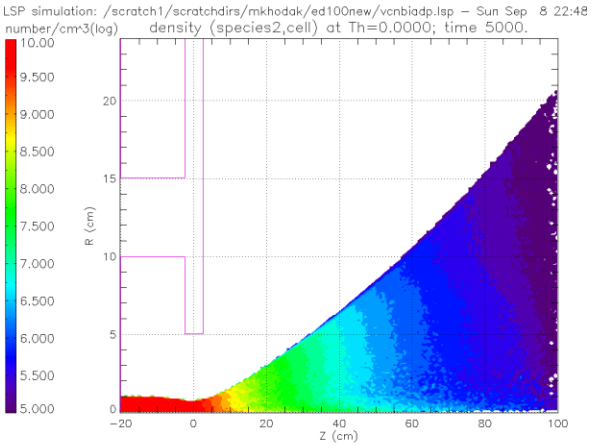

Figure 8

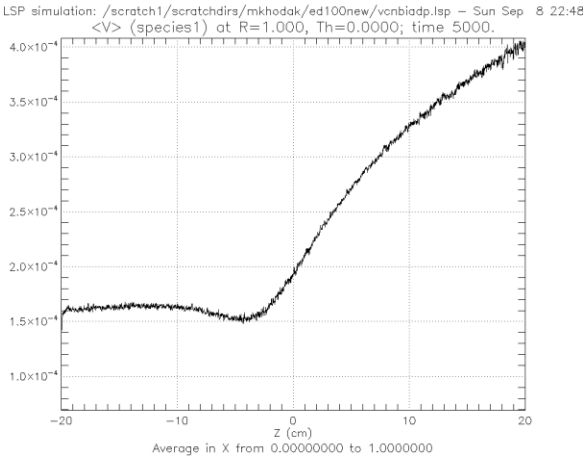

Figure 9

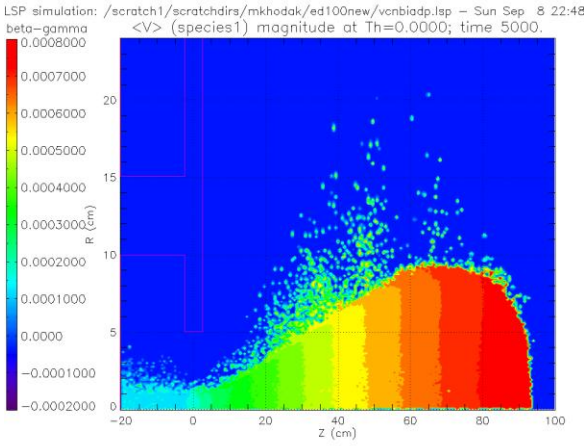

Figure 10

Case 2: Injecting Ions and Electrons at Thermal Velocity

This scenario used the same ion injection as before, although the velocity was changed to be the ion thermal velocity, $v_{T_i} = 2.19 \cdot 10^6 \frac{cm}{s}$. In this simulation, the electrons were also injected from the left side out to a radius of $1cm$, with a temperature of $20eV$ and a velocity of $1.87738 \cdot 10^8 \frac{cm}{s}$. A particle creation scheme of this sort was used to create a more realistic model by giving both particle species an initial axial momentum. Although particle injection density was set to $10^{10} cm^{-3}$, as the simulation progressed the density of both electrons and protons fell off to $2 \cdot 10^9 cm^{-3}$ before the nozzle and $2.6 \cdot 10^9 cm^{-3}$ at the nozzle (Figure 11).

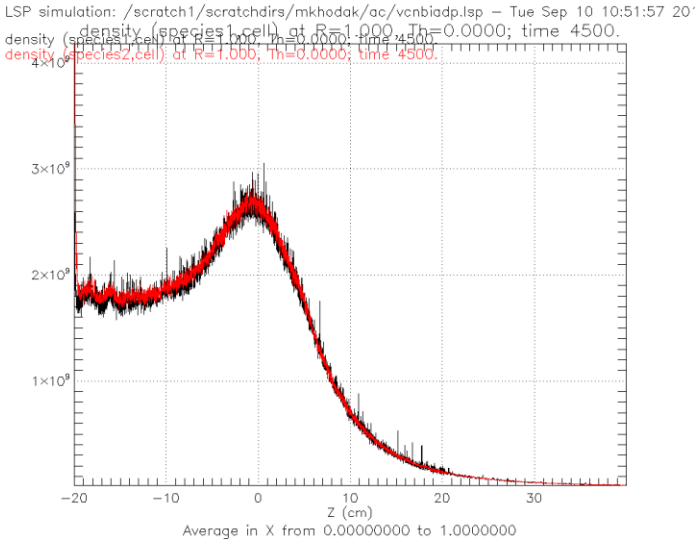

Figure 11

Although ion injection speeds were approximately 3 times slower than in the previous case, by $4500ns$, when the main density of ions had reached the nozzle, the dense ions upstream from the nozzle had a velocity of $1.23 \cdot 10^7 \frac{cm}{s}$, or twice the sound speed, and at the nozzle was $1.02 \cdot 10^7 \frac{cm}{s}$, slower than predicted by (5) if using an initial velocity of $1.23 \cdot 10^7 \frac{cm}{s}$ (Figure 12). Correspondingly, the potential at $1\mu s$ is approximately 3 times more negative than that shown in Figure 6 for the previous case (Figure 13). This larger negative potential and thus large ion acceleration is likely a result of the use of an initial electron momentum, allowing a greater density of them to concentrate ahead of the ions. In addition, in this simulation the minimal velocity occurs as expected at the nozzle throat, where B is greatest.

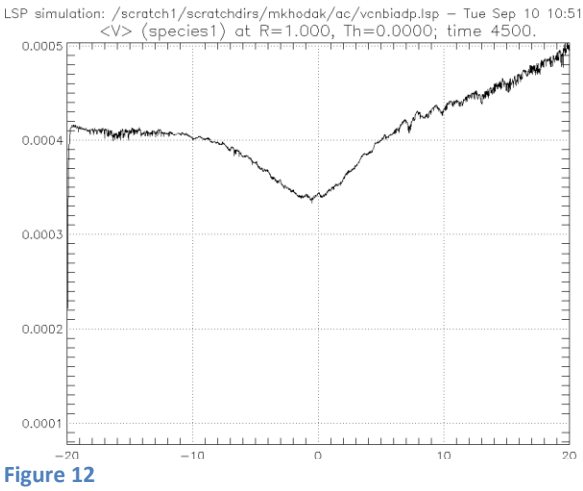

Figure 12

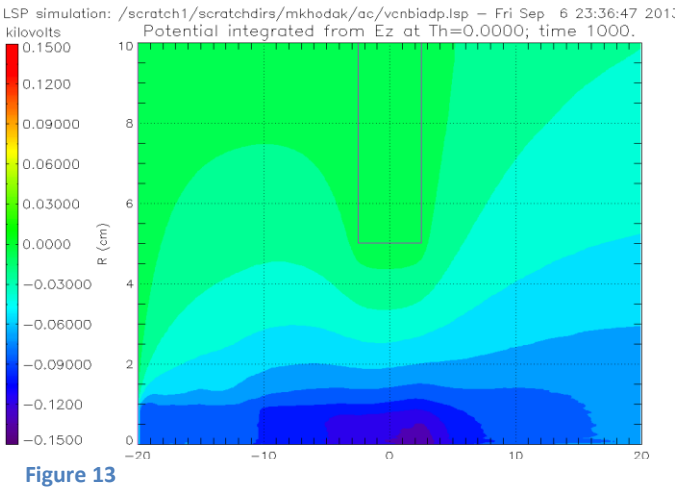

Figure 13

Nevertheless, as in Figures 7 and 8 in the previous case, the ions begin to seemingly detach from the field lines after $z = 40cm$, such that the behavior of ions at $4.5\mu s$ in this case is very similar to that at $5\mu s$ in the first case (Figure 14). However, the ions get to somewhat larger velocities at lower densities, reaching speeds corresponding to around $350eV$ (Figure 15). The simulations for Case 2 are also continuing to be conducted in order to examine electron behavior as ions move further downstream.

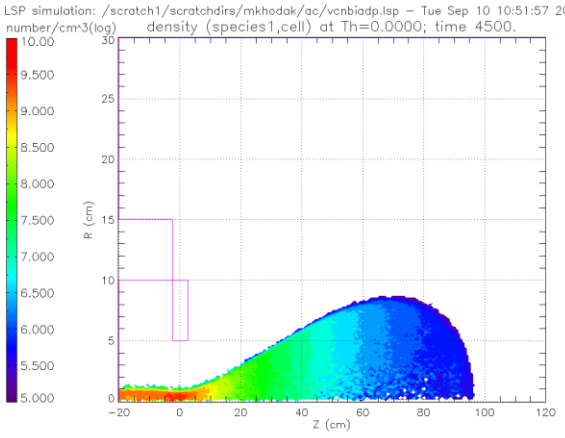

Figure 14

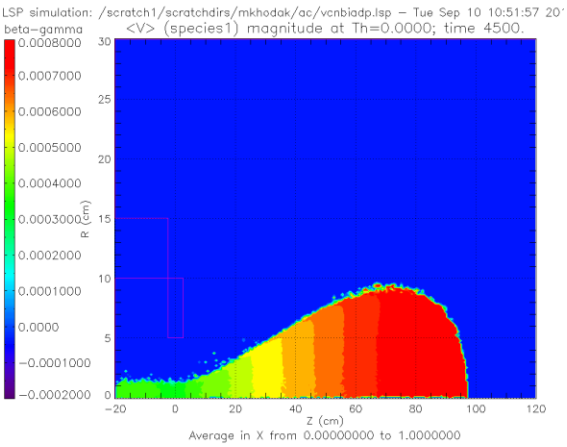

Figure 15

Computational Comparison

The Child-Langmuir model used approximately 10 macroparticles per cell at injection, although this was reduced by the particle collapse algorithm in LSP. Nevertheless, it still used 3 times fewer macroparticles than the two injection model, which also used particle collapse and the similar number of discrete particles for ions at injection. Likely as a result, the second model ran approximately twice as fast as the first. Despite using fewer particles, however, if one compares Figure 7 and Figure 14 one sees that the second run has fewer density gaps in the expansion region, and if one compares Figure 10 and Figure 15 one also sees fewer particles escaping from the main density region in the double-injection model. These observations point to the importance of resolving the grid spacing for the Debye length; while both simulations used the same grid spacing, which was $.01cm$ in both width and height at the nozzle and in the injection region, as well as the same timestep at $\Delta t = .01ns$, the first model had a denser plasma with a Debye length of $.037cm$ while the second had $\lambda_D = .073cm$. Since resolving the Debye length in LSP requires a grid spacing at least 5 times smaller, only the second simulation was fully resolved.

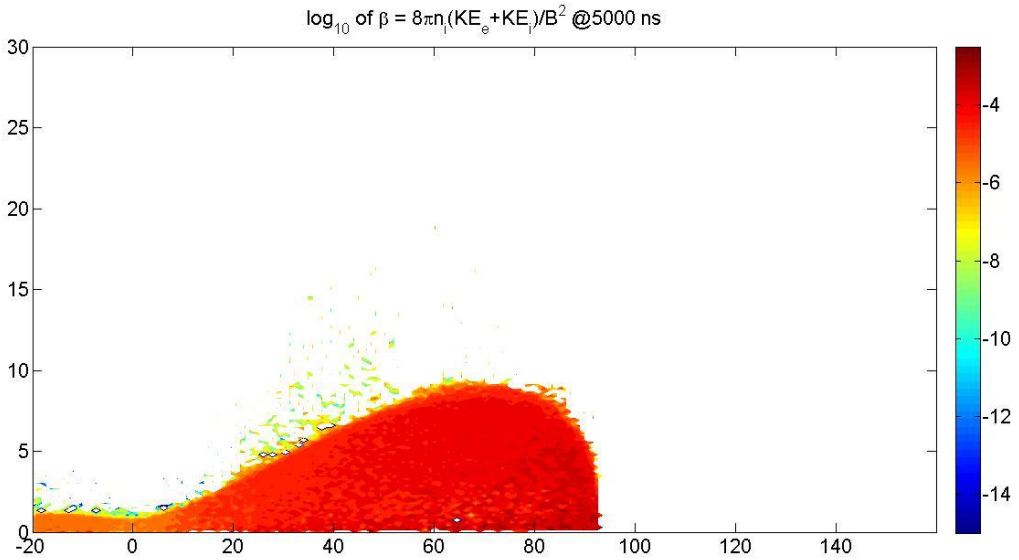

Figure 16

-plot generated by Aidan MacDonaugh

Conclusion and Further Study

These low density simulations are both important preliminaries for future work using denser plasmas. From them we know what to look for in the initial stages of detachment and can see indicators of ion acceleration downstream due to the constancy of the magnetic moment and their increasing parallel velocity. Future work in this area will involve continuing these simulations until a steady state is reached and then using what we have learned to move towards higher densities and higher β-levels from the current levels of $10^{-4} - 10^{-3}$ (Figure 16), using initial electron temperatures of 100eV and eventually getting to a target density of $10^{13} cm^{-3}$, a plasma density whose Debye length will need to be resolved at least 10 and ideally 30 times finer than the current resolution, which implies a 100 to a 1000-fold increase in the number of cells. Such simulations, while computationally intensive, will give us a clearer picture of detachment in practical plasma applications.

Project Supervisor:

-Samuel Cohen, PPPL

Acknowledgements:

-Dale Welch, Voss Scientific

-Aidan MacDonagh, Princeton University

References:

[1] A.V. Arefiev and B.N. Breizman, Phys. Plasmas **12**, 043504 (2005)